Structure of a DNA Glycosylase Searching for Lesions

Anirban Banerjee,[1] Webster L. Santos,[1] Gregory L. Verdine[1,2]*

DNA glycosylases must interrogate millions of base pairs of undamaged DNA in order to locate and then excise one damaged nucleobase. The nature of this search process remains poorly understood. Here we report the use of disulfide cross-linking (DXL) technology to obtain structures of a bacterial DNA glycosylase, MutM, interrogating undamaged DNA. These structures, solved to 2.0 angstrom resolution, reveal the nature of the search process: The protein inserts a probe residue into the helical stack and severely buckles the target base pair, which remains intrahelical. MutM therefore actively interrogates the intact DNA helix while searching for damage.

One of the most formidable needle-in-a-haystack challenges in biology is that faced by DNA glycosylases as they locate and excise damaged DNA nucleobases embedded in a greater than millionfold excess of undamaged DNA (*1*, *2*). The challenge is compounded by the fact that many damaged bases targeted by DNA glycosylases are only subtly different from their normal counterparts; for example, the highly mutagenic lesion 8-oxoguanine (oxoG) differs from G by only two atoms, and these modest alterations give rise to no major structural or energetic aberrations in the DNA helix (*3*–*5*). Because DNA glycosylases consume no biochemical energy during the search for damage, they must rely solely on thermally driven translocation along vast expanses of the genome. These constraints on the search process, plus the deleterious biologic effects of the failure to repair genotoxic lesions, have forced DNA glycosylases to evolve an exceptionally efficient means of interrogating DNA. Despite widespread speculation (*1*, *2*, *6*, *7*), the biophysical underpinnings of the process remain poorly understood (*8*, *9*).

The structure of the lesion recognition complex (LRC) comprising MutM, a bacterial DNA glycosylase specific for oxoG, bound to oxoG-containing DNA has revealed that MutM extrudes the damaged nucleotide from the DNA helix and inserts it into an active-site pocket on the enzyme (*10*) (Fig. 1A). Despite having no structural relationship to MutM, the eukaryotic functional counterpart of MutM, Ogg1, uses the same extrahelical strategy for oxoG recognition and repair (*11*). Indeed, an extensive body of diverse LRCs (*7*, *12*, *13*) strongly suggests that all DNA glycosylases operating on single-base lesions in the genome perform extrahelical base excision.

These studies leave unresolved the question of whether these enzymes search for lesions by actively extruding every base from DNA and presenting it for inspection to the active site. The energetic demands of such an extrahelical search would seem prohibitive. Alternatively, the active sites of DNA glycosylases might simply capture lesion bases that have undergone spontaneous extrusion from the DNA helix. Evidence has been presented that uracil DNA glycosylase uses such an extrahelical capture mechanism (*9*), but such a mechanism has not been demonstrated for other systems. Yet another plausible mechanism for lesion searching entails recognition of lesions by the DNA glycosylase while they still lie within the DNA helix (*14*), thus triggering extrusion and presentation to the active site. This option, intrahelical lesion recognition, is in many respects the most kinetically tenable, yet the structural basis for such recognition remains obscure.

Recently, intermolecular disulfide cross-linking (DXL) technology has been used to capture human 8-oxoguanine DNA glycosylase (hOGG1) in the act of extruding a normal nucleobase from DNA (*8*). To capture earlier intermediates in DNA interrogation, we focused on the bacterial counterpart of hOGG1, MutM, which has been the subject of extensive biochemical (*14*–*17*) and structural (*10*, *18*–*21*) analysis. Here, we describe the use of DXL to obtain multiple structures of MutM performing an invasive interrogation of an undamaged DNA helix. These structures illuminate an early stage of the search process and suggest that oxoG lesions are located by intrahelical interrogation.

We identified several potential sites for DXL in the protein-DNA interface of the *Bacillus stearothermophilus* MutM LRC (Fig. 1) (*10*). MutM variants containing single cysteines at the relevant positions were created, and oligonucleotides were synthesized (*22*–*25*) each containing a single thiol tether attached to the corresponding backbone phosphates (Fig. 1B). These thiol-tethered oligonucleotides were incubated with the respective MutM variants, and the extent of cross-linking was analyzed by SDS–polyacrylamide gel electrophoresis under non-reducing conditions (fig. S1). The combination that exhibited the most favorable time course (fig. S1) and furnished the cross-linked product in the highest yield and purity was Q166C/p9′ with a two-carbon (C2) tether. This complex (hereafter referred to as interrogation complex 1, IC1) was therefore selected for further investigation.

Diffraction-quality crystals of IC1 were obtained after substantial modifications of the conditions used to grow crystals of the LRC (*10*). Nonetheless, the IC1 crystals, which diffracted to 2.0 Å resolution, belonged to the same space group and had approximately the same unit cell dimensions as those of the LRC (see table S1 for data collection and refinement statistics). The structure of IC1 was solved by molecular replacement using the coordinates of the protein from the structure of the *B. stearothermophilus* MutM LRC (*10*).

Our cross-linking scheme was designed to elucidate the structural details of MutM interrogating a G:C base pair at the same position [Fig. 2, base pair 8 (bp8)] that was previously occupied by the oxoG:C base pair in the LRC. Surprisingly, inspection of the IC1 structure revealed that the protein was not interrogating the intended target G:C base pair, but instead had positioned itself on the DNA so as to interrogate the A:T base pair at bp9 (Fig. 2B, cyan). Evidently, the disulfide cross-link incorporated into this protein-DNA interface still allows sufficient freedom of movement for MutM to reposition itself by a full base pair step along DNA.

In the LRC, the oxoG lesion is extruded into the extrahelical enzyme active site, and the DNA helix is penetrated by three key residues on the enzyme (Figs. 2E and 3A). The aromatic ring of Phe^{114} is wedged into the helical stack to enforce a sharp bend in the DNA. The side chain of Arg^{112} extends into the space vacated by oxoG and forms hydrogen bonds with the Watson-Crick face of the estranged C. Met^{77} also fills the void in the DNA helix, making van der Waals contacts with the nucleobase on the 3′ side of the lesion and with the sugar of the nucleotide on the 5′ side.

The nature of the protein-DNA interaction in IC1 differs in one major respect from that previously determined for any DNA glycosylase complex, in that the target base pair in DNA is completely intact and fully intrahelical. Although intact, the target A:T base pair is buckled, probably as the result of the forced insertion of Phe^{114} into the helix directly above the Watson-Crick hydrogen bonds of the A:T pair (Fig. 3B). Whereas Phe^{114} serves an analogous role in IC1 and the LRC, Arg^{112} and Met^{77} do not. With no vacant space in the helix, the side chain of Arg^{112} is retracted from the DNA and points downward into the minor groove space, forming hydrogen bonds to the O4′ of G10 and G11 and the N3 atom of G10. The side chain of Met^{77} is rotated and no longer makes the same van der Waals contacts with the DNA, but the methyl group of Met^{77} does contact the sugar moiety of the target A. The loop containing Met^{77} is retracted from the DNA surface by ~1 Å relative to its position in the LRC, and this presumably serves

[1]Department of Chemistry and Chemical Biology, [2]Department of Molecular and Cellular Biology, Harvard University, Cambridge, MA 02138, USA.

*To whom correspondence should be addressed. E-mail: gregory_verdine@harvard.edu

to weaken the interactions between this residue and the DNA. The only notable conformational change in the protein is the loss of ordered structure in the prominent surface loop that makes four hydrogen bonds to the extrahelical oxoG in the LRC (*10*); in IC1 and in all other structures of interrogation complexes presented here (see below), this loop is completely disordered. This oxoG recognition loop is also disordered in all structures of MutM bound to postexcision intermediates (or analogs thereof) in the base-excision repair pathway (*19*–*21*) that no longer possess an oxoG nucleobase.

In an attempt to encourage MutM to interrogate the G:C base pair at position 8, we moved the cross-link attachment point from p6 to p5. The structure of the resulting complex revealed a pronounced overall helical distortion in the DNA that enabled MutM to continue interrogating the A:T base pair at position 9 (+4 register) (*26*). This observation indicates a preference on the part of MutM to interrogate A:T base pairs rather than G:C. To test the notion that the induced duplex distortion results from an aversion to interrogate a G:C pair, we mutated bp8 to A:T while maintaining the tether attachment point at p5 and solved the structure of the cross-linked complex (hereafter referred to as interrogation complex 2, IC2) to 2.0 Å resolution. In this structure (Fig. 2C) (fig. S2), MutM adopts the +3 register on DNA and interrogates the A:T base pair at position 8 in the duplex. The conformation of the DNA flanking the target base pair is typical B form. Thus, changing the G:C base pair at position 8 to A:T alleviates the aversion to interrogating bp8 and relieves the attendant helical distortion. Even though MutM is slid by one base pair along the duplex in IC1 versus IC2, the overall helical structure and local interactions at the site of helix penetration by Phe[114] are remarkably similar in the two complexes (Fig. 2F) (figs. S3 and S4).

To capture MutM interrogating a G:C base pair, we swapped the G:C and A:T base pairs at bp7 and bp9 in the IC1 DNA, thereby presenting the protein with a stretch of DNA containing only G:C pairs in the +2, +3, and +4 registers. We crystallized this complex (IC3) and solved its structure to 2.05 Å resolution. Inspection of the structure of IC3 reveals MutM to be bound over DNA in the +3 register, interrogating a fully intrahelical G:C base pair at position 9 in the duplex (Figs. 2D and 3C) (fig. S3). Notwithstanding the aforementioned aversion of the protein to interrogate G:C base pairs, the resulting structure (Fig. 3C) is strikingly similar to that of the A:T interrogation complexes, with a severely buckled base pair at the site of helix penetration by Phe[114], and with Arg[112] and Met[77] lying in wait (see fig. S4 for details of the buckling parameters).

The structure of the LRC (*10*) revealed a duplex structure with a sharp bend (~80°) at the site of the lesion, enforced through extensive interactions with the DNA backbone of both the lesion-containing and non–lesion-containing strands. To what extent are these interactions maintained or disturbed in the interrogation complexes? To answer this question, we solved structures of control cross-linked LRCs (E3Q, Q166C MutM) having oxoG:C in place of the non–lesion-containing target base pair in IC1 and IC3 (control complex 1, CC1), or in IC2 (CC2) (figs. S3 and S5). The structure of CC2 superimposes on the LRC with an overall heavy-atom root mean square deviation (RMSD) of 0.250 Å, and CC2 exhibits no apparent structural distortion at the site of tether attachment; CC1 also compares similarly well with the same complex lacking a cross-link (*27*), thus demonstrating the absence of any discernible cross-link–induced structural perturbation.

The overall positioning of DNA with respect to the surface of MutM, and the extent and locus of DNA bending, is so similar in the LRCs and the interrogation complexes (Fig. 2, E and F) (fig. S3) that a close inspection is required to discern the differences between them. The pronounced overall similarity of IC1,

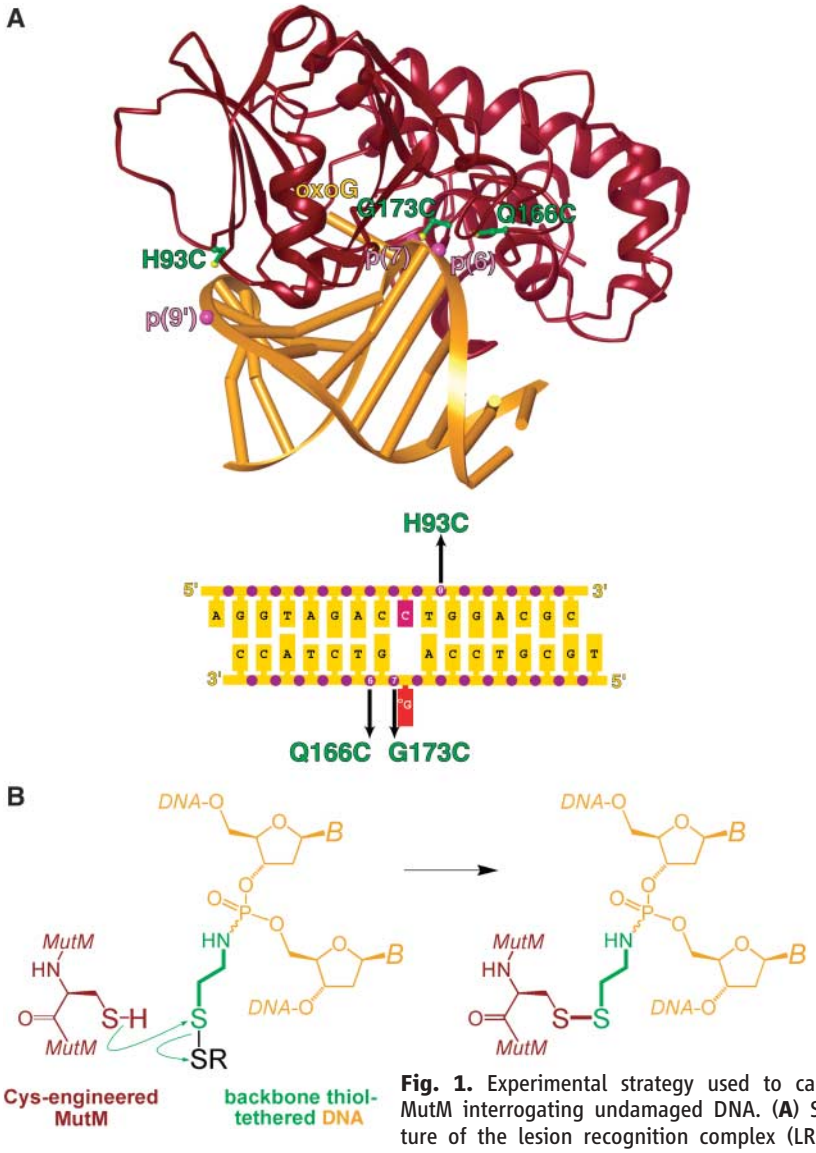

Fig. 1. Experimental strategy used to capture MutM interrogating undamaged DNA. (**A**) Structure of the lesion recognition complex (LRC) of MutM (crimson) bound to oxoG-containing DNA (gold). The side chains of Cys residues introduced individually are shown in green, with nearby backbone phosphates shown in magenta. The schematic sequence diagram below the structure illustrates the relationship of the cross-linking sites in DNA to the positions of the oxoG lesion and its complementary C (the "estranged" C). Abbreviations for amino acids: C, Cys; G, Gly; H, His; Q, Gln. (**B**) Structure of the N-thioalkyl phosphoramidate moiety substituted for a backbone phosphate (thiol-containing tether in green, DNA backbone in yellow); wavy line indicates a mixture of two diastereomers at phosphorus. Only the C2 linker is shown; homologation by the insertion of one or two additional $-CH_2-$ groups into the linker gives C3 and C4, respectively. Also shown is the chemical structure of the starting materials and products of the cross-linking reaction; curved arrows denote electron flow in the cross-linking reaction.

IC2, and IC3 with MutM LRCs supports the notion that the interrogation complexes described here represent an early intermediate (*28*) in the base extrusion pathway used by MutM to search for lesions in DNA and present them to the extrahelical active site.

Closer inspection of the structures, however, reveals a substantial but highly localized structural reorganization concomitant with lesion recognition. The energetically favorable (*29*) transition from a nonlesion interrogation complex to a lesion-specific recognition complex entails conformational rearrangements that are localized almost exclusively to the interface between MutM and the target strand. Most noteworthy is the wholesale replacement of multiple direct backbone contacts to the target strand in CC2, CC1, and LRC with an extensive array of indirect contacts involving ordered bridging water molecules (Fig. 4) (fig. S6). The swiveling motion about phosphates flanking the lesion nucleoside that accompanies helical extrusion appears to reposition them from a conformation favoring water-mediated backbone contacts to one favoring direct contacts. The oxoG appears to exit the duplex from the minor groove side, opposite to what has been proposed for hOGG1 (*8*). Although the precise details of the contact repertoire differ among IC1, IC2, and IC3, all share the overall similarity of using an extensive array of water-mediated contacts, plus a few direct contacts, instead of the mostly direct contacts seen in the lesion-specific complexes. In this respect, the transition from an interrogation complex to a lesion-specific complex in the case of MutM is accompanied by the same decrease in solvation at the protein-DNA interface that was documented for sequence-specific DNA binding proteins bound to noncognate versus cognate DNA sequences (*30*–*34*). These interfacial waters most likely provide a form of lubricant to facilitate fast sliding of the protein along normal DNA.

Notwithstanding the local differences noted above in protein-DNA interactions between the structures of MutM bound to damaged DNA and to non–lesion-containing DNA (IC1, IC2, and IC3), one prominent feature emerges as being common to all of these complexes. In these and all other structures of MutM and its orthologs bound to DNA (*10*, *18*–*21*), Phe^{114} is inserted into the DNA duplex, and this is accompanied by nearly complete loss of helix stacking at the site of intercalation. Furthermore, in normal DNA, insertion of Phe^{114} is associated with the buckling of a target base pair at the intercalation site. Buckled base pairs are intrinsically less stable than canonical pairs; hence, Phe^{114} can be seen to cause a highly localized destabilization of the target base pair. This implies that Phe^{114} can act as a sensor for the deformability of base pairs in DNA. Stated otherwise, intercalation of Phe^{114} imposes a specific structural and energetic test on the tar-

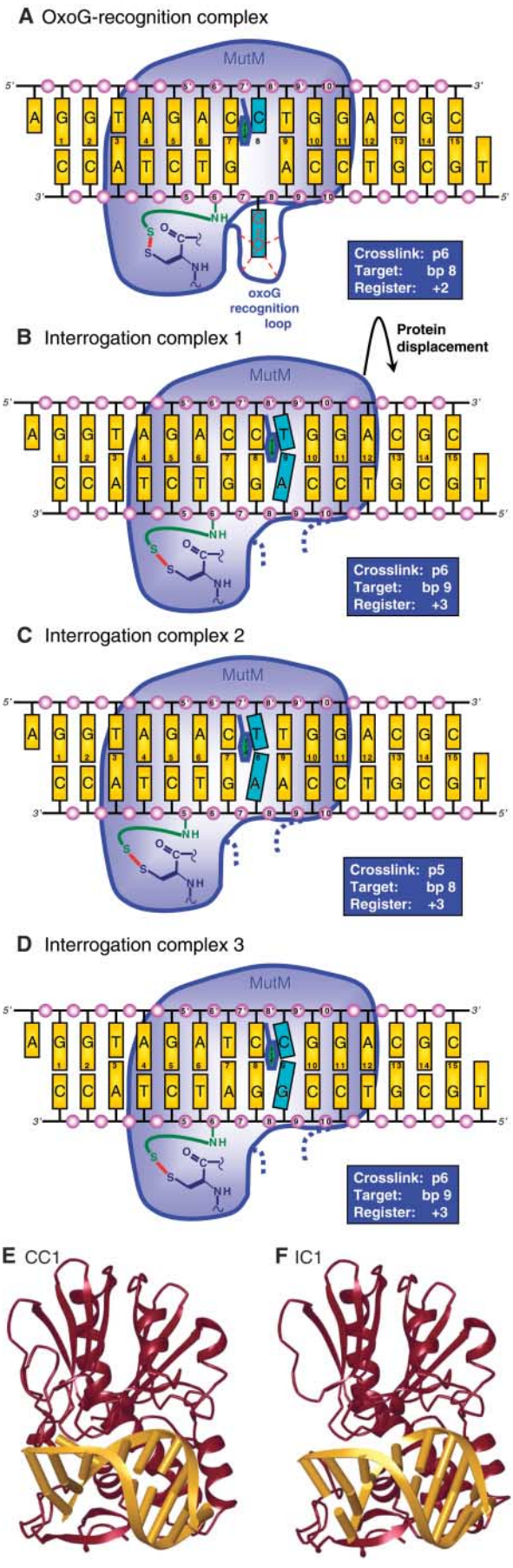

Fig. 2. Schematic representation of MutM-DNA complexes. (**A**) The MutM LRC used as the basis for the design of the cross-linking system. (**B** to **D**) Interrogation complexes showing the positioning of MutM over the DNA duplex, with the target base pair in aqua. The side chain of the helix-probe residue Phe^{114} is indicated. The numbering system for the base pairs and backbone phosphates is as indicated. The curved green line denotes the thiol-bearing tether engaged in a cross-link to Cys^{166}. Each blue box indicates the site of tether attachment to DNA, the position of the target base pair, and the separation between them, here referred to as the register. Dashed blue lines indicate the lack of order in the oxoG recognition loop. (**E** and **F**) Overall view of complexes CC1 (E) and IC1 (F). CC1 is a lesion recognition complex (LRC) formed by disulfide cross-linking between MutM and oxoG-containing DNA. IC1 is the corresponding interrogation complex having MutM cross-linked to non–lesion-containing DNA. Blue box denotes the target base pair, which is disrupted in (E) and intact but buckled in (F).

get base pair in DNA. Although the destabilizing effect of Phe^{114} insertion may well be below the magnitude that can be observed in nuclear magnetic resonance experiments measuring imino proton exchange rates (*9*), they could nonetheless make an important contribution to the lesion-searching process and base extrusion pathway. It is noteworthy that in the structure of unliganded MutM, both the side chain of Phe^{114} and the protein backbone in the region surrounding this residue are highly constrained conformationally, as judged by inspection of the structure (fig. S7) and by the lower temperature factors (*B* factors) for this region than for the average residue. Insertion of Phe^{114} thus appears to arise as an unavoidable consequence of formation of an intimate DNA-bound complex by MutM. The structures of LRCs bearing DNA glycosylases from diverse superfamilies (fig. S8) all reveal a helix-intercalating probe residue, which suggests that this strategy may be widely used to test the structure and energetics of base pairs in DNA while searching for lesions.

The present structures suggest a means by which MutM, and by extension hOGG1, may be able to sense the presence of oxoG residues in an intact DNA helix (intrahelical lesion recognition). Even though oxoG:C base pair has no discernible effect on the conformation of duplex DNA (*3*, *4*) and has only slightly weaker pairing than A:T (*5*), perhaps oxoG:C behaves differently from A:T and G:C when subjected to interrogation by the intercalating probe residue. Taking into account the fact that the lesion search process is Brownian and therefore highly redundant, it is less critical that the enzyme recognize an oxoG lesion upon every encounter, because the enzyme will have many additional opportunities to identify the lesion. What is important is that the enzyme minimizes the incidence of a time-intensive interrogation of nonlesion base pairs in normal DNA. This realization leads to two additional important notions: (i) Negative selection against extruding bases from normal DNA may be at least as important for lesion recognition as positive selection for extrusion of oxoG lesions. As shown here, MutM clearly exhibits an aversion to intercalative probing of G:C base pairs, suggesting at least one way in which negative selection

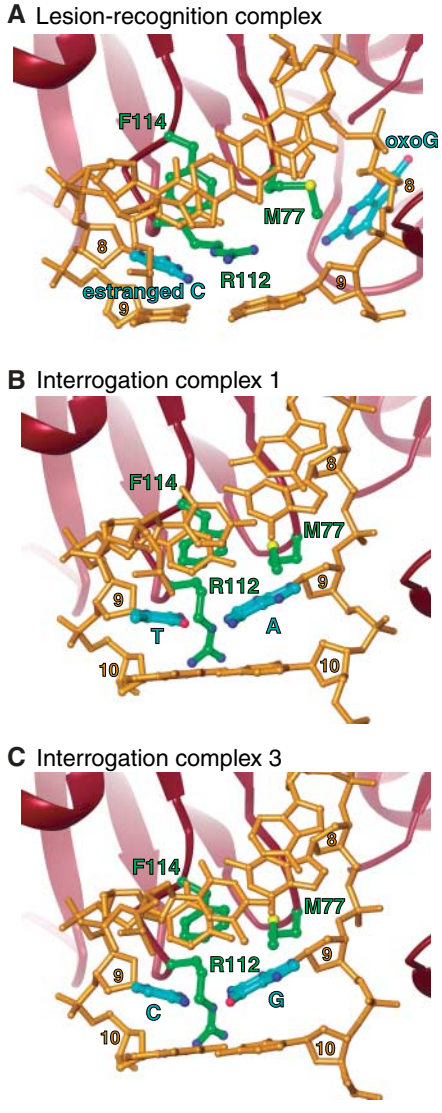

Fig. 3. Close-up views of key interactions in the MutM-DNA interface. (**A**) The control cross-linked LRC CC2; (**B**) IC1; (**C**) IC3. The protein backbone is in a crimson ribbon representation, with the side chain of key residues shown in green. The DNA is in a yellow framework model, with the target base pair in aqua. The target base pair is broken in (A) by extrusion of oxoG from the helix and insertion into the active-site pocket; the target base pair in (B) and (C) is intact but severely buckled. Abbreviations for amino acids: F, Phe; R, Arg; M, Met.

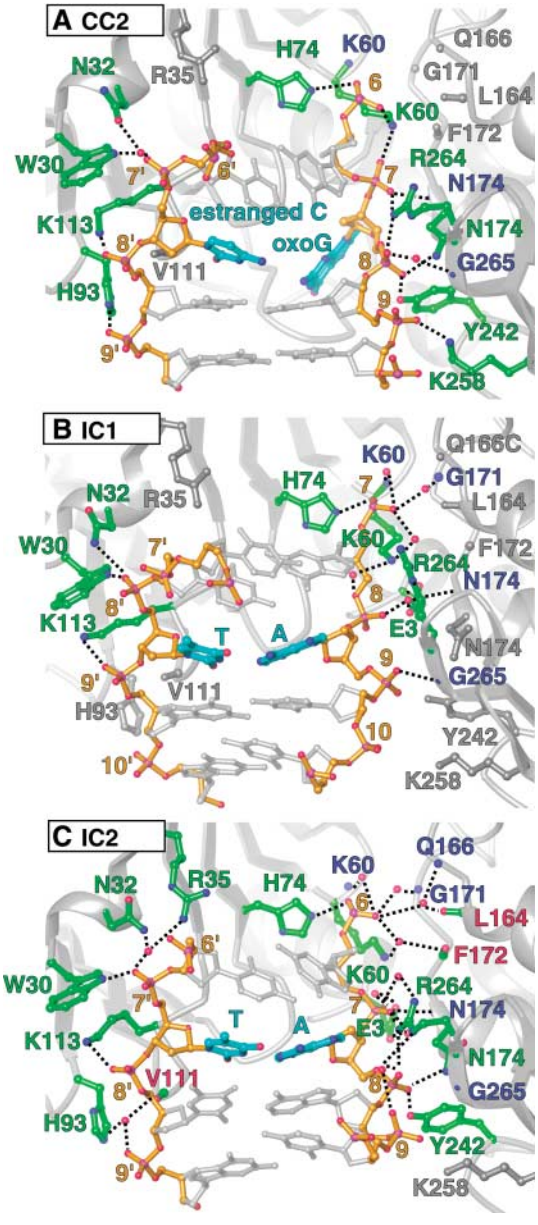

Fig. 4. Direct and water-mediated interactions between MutM and the DNA backbone in the control LRC CC2 (**A**) and interrogation complexes IC1 (**B**) and IC2 (**C**). Dashed lines indicate hydrogen bonding interactions among backbone phosphates in DNA, ordered waters (red spheres), and residues in MutM. The side chains of amino acid residues are shown in green with the numbers colored according to which moiety on the amino acid is involved in the contact: green, side chain; blue, backbone amide NH; red, backbone amide carbonyl; gray, no contact in that particular complex.

can be achieved. (ii) Lesion discrimination seems to result from a kinetic preference to extrude oxoG residues from the DNA helix, relative to normal bases. Should the enzyme occasionally make a mistake and attempt to present a normal base to the active site, that poses no danger, as we have shown, in the case of hOGG1, that the active site has an exquisite ability to discriminate thermodynamically in favor of oxoG (*8*).

References and Notes

1. G. L. Verdine, S. D. Bruner, *Chem. Biol.* **4**, 329 (1997).
2. D. O. Zharkov, A. P. Grollman, *Mutat. Res.* **577**, 24 (2005).
3. L. A. Lipscomb *et al.*, *Proc. Natl. Acad. Sci. U.S.A.* **92**, 719 (1995).
4. Y. Oda *et al.*, *Nucleic Acids Res.* **19**, 1407 (1991).
5. G. E. Plum, A. P. Grollman, F. Johnson, K. J. Breslauer, *Biochemistry* **34**, 16148 (1995).
6. S. S. Parikh, C. D. Putnam, J. A. Tainer, *Mutat. Res.* **460**, 183 (2000).
7. J. T. Stivers, *Prog. Nucleic Acid Res. Mol. Biol.* **77**, 37 (2004).
8. A. Banerjee, W. Yang, M. Karplus, G. L. Verdine, *Nature* **434**, 612 (2005).
9. C. Cao, Y. L. Jiang, J. T. Stivers, F. Song, *Nat. Struct. Mol. Biol.* **11**, 1230 (2004).
10. J. C. Fromme, G. L. Verdine, *J. Biol. Chem.* **278**, 51543 (2003).
11. S. D. Bruner, D. P. Norman, G. L. Verdine, *Nature* **403**, 859 (2000).
12. J. C. Fromme, G. L. Verdine, *Adv. Protein Chem.* **69**, 1 (2004).
13. J. L. Huffman, O. Sundheim, J. A. Tainer, *Mutat. Res.* **577**, 55 (2005).
14. J. Tchou *et al.*, *J. Biol. Chem.* **269**, 15318 (1994).
15. M. Bhagwat, J. A. Gerlt, *Biochemistry* **35**, 659 (1996).
16. S. Boiteux, T. R. O'Connor, F. Lederer, A. Gouyette, J. Laval, *J. Biol. Chem.* **265**, 3916 (1990).
17. D. O. Zharkov, R. A. Rieger, C. R. Iden, A. P. Grollman, *J. Biol. Chem.* **272**, 5335 (1997).
18. F. Coste *et al.*, *J. Biol. Chem.* **279**, 44074 (2004).
19. J. C. Fromme, G. L. Verdine, *Nat. Struct. Biol.* **9**, 544 (2002).
20. R. Gilboa *et al.*, *J. Biol. Chem.* **277**, 19811 (2002).
21. L. Serre, K. Pereira de Jesus, S. Boiteux, C. Zelwer, B. Castaing, *EMBO J.* **21**, 2854 (2002).
22. The oligonucleotides were synthesized using an automated synthesis procedure based on established chemistry (*23*–*25*). The synthesis was carried out on an ABI 392 synthesizer by modifying a regular 1 μM scale synthesis protocol to perform an H-phosphonate coupling step, followed by oxidation using carbon tetrachloride and diamine disulfide (free base) at the site of tether incorporation. (See the supplementary material for additional details.)
23. F. R. Atherton, H. T. Openshaw, A. R. Todd, *J. Chem. Soc.* **1945**, 660 (1945).
24. B. C. Froehler, M. D. Matteucci, *Tetrahedron Lett.* **27**, 469 (1986).
25. R. L. Letsinger, M. E. Schott, *J. Am. Chem. Soc.* **103**, 7394 (1981).
26. A. Banerjee, G. L. Verdine, unpublished data.
27. A. Banerjee, W. L. Santos, G. L. Verdine, data not shown.
28. O. S. Fedorova *et al.*, *Biochemistry* **41**, 1520 (2002).
29. A. A. Ishchenko *et al.*, *Biochemistry* **41**, 7540 (2002).
30. D. T. Gewirth, P. B. Sigler, *Nat. Struct. Biol.* **2**, 386 (1995).
31. C. He *et al.*, *Mol. Cell* **20**, 117 (2005).
32. C. G. Kalodimos *et al.*, *Science* **305**, 386 (2004).
33. H. Viadiu, A. K. Aggarwal, *Mol. Cell* **5**, 889 (2000).
34. F. K. Winkler *et al.*, *EMBO J.* **12**, 1781 (1993).

35. Supported by NIH grant GM044853. For help during data collection and processing, we thank M. Becker and all the staff members at National Synchrotron Light Source beamline X25; C. Heaton, B. Miller, and staff members at Chess A1 beamline; and C. Ogata and N. Sukumar at APS 8BM beamline. We also thank Y. Korkhin for help and advice; Enanta Pharmaceuticals for use of their x-ray facilities for initial characterization of the crystals; and C. Fromme, P. Blainey, and M. Spong for discussions and suggestions on the manuscript. Coordinates and structure factors have been deposited in the Protein Data Bank with accession codes 2F5S (CC1), 2F5Q (CC2), 2F5N (IC1), 2F5P (IC2), and 2F5O (IC3).

Supporting Online Material

www.sciencemag.org/cgi/content/full/311/5764/1153/DC1
Materials and Methods
Figs. S1 to S8
Table S1

19 September 2005; accepted 18 January 2006
10.1126/science.1120288

Coherent Sign Switching in Multiyear Trends of Microbial Plankton

William K. W. Li,* W. Glen Harrison, Erica J. H. Head

Since the 1990s, phytoplankton biomass on the continental shelf of Nova Scotia and in the Labrador Sea has undergone sustained changes in the spring and fall, which are accompanied by changes in bacterioplankton that are dampened in amplitude but coherent in the direction of change. A reversal of trend in biomass change, so-called sign switching, occurs both in time and in space. Thus, whenever (spring or fall) and wherever (Scotian Shelf or Labrador Sea) phytoplankton increase or decrease, so also does bacterioplankton. This tandem sign switch indicates coupling of the trophic levels at a multiyear time scale and contributes to an ecological fingerprint of systemwide forcing.

Sustained monitoring of large ocean ecosystems often reveals systematic changes in phytoplankton abundance. These have been ascribed to systemwide influences such as climate change (*1*) and removal of top predators (*2*). Changes at one trophic level may cascade up or down the food web, and the effects may be discerned when other trophic levels are also monitored (*3*). A large proportion (about 50%) of primary production is routed through the microbial loop in which heterotrophic bacterioplankton assimilate or respire the substrates originating from phytoplankton (*4*). It might thus be inferred that a long-term change in phytoplankton would lead to a concomitant change in bacterioplankton, but we are not aware of any direct evidence at the appropriate time scale.

Here, we show that since the 1990s, phytoplankton biomass on the continental shelf of Nova Scotia and in the Labrador Sea has undergone sustained changes that are accompanied by changes in bacterioplankton, dampened in amplitude but coherent in the direction of change. A reversal of trend in biomass change, so-called sign switching (*5*), occurs both in time (between seasons) and in space (among locations), and the two trophic groups switch sign in tandem. Although heterotrophic and photoautotrophic plankton interact at the short scales of microbial generation times and cellular distances, the ecological relationship between these two trophic groups (at the large scales of a decade and ocean shelves) appears responsive to systemwide forcing.

The Scotian Shelf (SS) has been sampled every spring (April and May) and every fall (October) since 1997 along a western (WSS), a central (CSS), and an eastern (ESS) section, with seven stations on each section comprising the core element of the Canadian Atlantic Zone Monitoring Program (*6*). Additionally, at a single CSS station (HL2, 44.27°N, 63.32°W), there is supplementary sampling once every 2 weeks to delineate higher frequency events. The Labrador Sea has been sampled every spring or early summer (May to July) since 1994 on 28 stations along a section (*7*) starting from Hamilton Bank on the Labrador Shelf (LS), through the central deep Labrador Basin (LB), and ending at Cape Desolation on the Greenland Shelf (GS). At each of the 49 hydrographic stations (fig. S1), we monitor chlorophyll concentration and bacterioplankton abundance (*8*) from the sea surface to 100 m and compute depth-integrated standing stocks of both biotic components. Semimonthly values of surface chlorophyll are also computed throughout the study region with the use of satellite ocean color imagery (*8*).

The biweekly record of depth-integrated chlorophyll concentration at HL2 shows repeated cycles of a major bloom in spring and a minor bloom in fall (Fig. 1A). Over 6 years, average spring chlorophyll (March to May) has been increasing at 14% per year while average fall chlorophyll (September to November) has been decreasing at –9% per year. The same directions of change are also evident in the remotely sensed record of surface chlorophyll (Fig. 1B), abundance of diatoms (Fig. 1C), and abundance of dinoflagellates (Fig. 1D), but with only weak or no statistical significance in all of them (table S1).

Bedford Institute of Oceanography, P.O. Box 1006, Dartmouth, Nova Scotia B2Y 4A2, Canada.

*To whom correspondence should be addressed. E-mail: LiB@mar.dfo-mpo.gc.ca